# A wide bandgap metal-free perovskite for third-order nonlinear optics

Dumitru Sirbu,[†] Hei Chit Leo Tsui,[*,†] Naseem Alsaif,[†,‡] Susana Iglesias-Porras,[†] Yifeng Zhang,[¶] Ming Wang,[¶] Mingzhen Liu,[¶] Anna C. Peacock,[§] Pablo Docampo,[†] and Noel Healy[†]

[†]*Emerging Technologies and Materials Group, School of Mathematics, Statistics and Physics, Newcastle University, Newcastle, NE17RU, UK*

[‡]*Department of Physics, Faculty of Science, Jazan University, Jazan, Saudi Arabia*

[¶]*School of Materials and Energy, Center for Applied Chemistry, University of Electronic Science and Technology of China, Chengdu, 611731, P. R. China*

[§]*Optoelectronics Research Centre, University of Southampton, Southampton, SO171BJ, UK*

E-mail: hei.tsui@newcastle.ac.uk

**Abstract**

This paper establishes the potential of the recently introduced $ABX_3$ metal-free perovskite structures for third-order nonlinear optical processes. The base unit in this family of materials is an ammonium halide octahedra and it incorporates a large aromatic cation spacer forming the classic perovskite structure. This work shows that the choice of cation is key to the resulting third order nonlinearity, where incorporation of 'MDABCO' into the structure, a very polar cation, results in a third order nonlinear refractive index on the order of $10^{-17}\,\mathrm{m^2\,W^{-1}}$ and high laser damage threshold of $0.8\,\mathrm{J\,cm^{-2}}$. Owing to its very wide bandgap of $\sim$5.12 eV, this material exhibits a high nonlinear figure of merit across the visible and near infrared transmission windows.

These results show that the metal-free family of perovskite materials is an excellent candidate for nonlinear optics in the important visible and near-infrared wavelength regimes.

**keywords:** third-order susceptibility, nonlinear absorption, nonlinear refraction, Kerr, $z$-scan, damage threshold**keywords:** third-order susceptibility, nonlinear absorption, nonlinear refraction, Kerr, $z$-scan, damage threshold

# Introduction

Owing to their superlative photovoltaic and luminescent properties, hybrid halide perovskites have attracted a great deal of attention for solar cell and light-emitting diode applications.[1,2] Critically, their optoelectronic properties can be easily tuned by simple modifications to the crystal structure,[3] which is based an $ABX_3$ configuration; where A is typically a monovalent cation, B is a divalent metal, and X is a halide. For example, the bandgap energy can be tuned in the range of 3 eV to 1.5 eV by partial or complete substitution of the halide anion.[4] The large bulk of the extensive research into perovskites has been at or above the bandgap energy as these are the important energies for photovoltaic and light emission applications. More recently, hybrid halide perovskites have been explored for optical applications at sub-bandgap energies and now a new application space has emerged; the field of nonlinear optics.[5–9]

Since its first demonstration in 1961 by Franken *et al.*,[10] nonlinear optics has grown, not only to be an important field in its own right, but also as a key enabling technology that has underpinned major breakthroughs in many cutting edge applications, such as, quantum optics, telecommunications, and super-resolution microscopy. In general, it is the second- and third-order susceptibilities that are exploited for nonlinear optical technologies. Second-order processes include second harmonic generation and are limited to materials

with non-centrosymmetric crystal structure. In contrast, all materials possess a third-order nonlinearity and it is this that is responsible for processes such as the optical Kerr effect and two-photon absorption. Preliminary investigations have shown that hybrid halide perovskites are very strong candidates to become an important platform for nonlinear optical devices. For example, the prototypical methylammonium lead iodide, $CH_3NH_2PbI_3$, (MAPI) shows a large third-order nonlinear response in the near-IR transmission window for both films and single crystals.[11–15] Indeed, a Kerr optical nonlinearity that is orders of magnitude greater than silicon, which is considered an important material for nonlinear optics, has been demonstrated, thus, highlighting the enormous potential for these materials.[12] However, many reports show that hybrid halide perovskites have a low laser induced damage threshold (LIDT), which may preclude their use for nonlinear applications that typically require high light intensities.[13,16,17] More critically, hybrid halide perovskites contain lead and that may ultimately be the limiting factor to their potential applications.[18–22]

The newly introduced metal-free perovskites[23] offer an exciting unexplored alternative, which addresses these toxicity and absorption concerns. Like the hybrid halide perovskites, this family of materials is based on the $ABX_3$ structure but, in contrast, the charge values in the A and B sites are interchanged, i.e. A is a divalent cation while B is a monovalent cation. These materials have recently been successfully implemented as efficient and stable ferroelectrics and have also been predicted to be suitable for second-order nonlinear optics, with simulations showing a high second-order susceptibility.[23,24] This work explores this new class of material as a potential platform for third-order nonlinear optics. Presented is the first experimental demonstration of the third-order nonlinear optical properties of metal-free perovskites. It is shown that incorporating a polar cation into the non-polar DABCO – NH4I3(DNI) system to produce Methyl-DABCO (MDNI), changes the crystal structure from a 1D hexagonal P62c perovskite structure with face-sharing octahedra to a corner-sharing 3D trigonal R3 perovskite structure with highly ammonium halide octohedra, Figure 1, and

a high third-order nonlinearity is produced. Here DABCO is defined as the dication 1,4-diazoniumbicyclo[2.2.2]octane that upon methylation produces the desymmetrized Methyl-DABCO (MDABCO). We benchmark these materials with MAPI, which is the archetypal lead-based perovskite. Our results show that the polar MDNI material has a nonlinear figure of merit of >500 at 1060 nm, which is more than four orders of magnitude greater than MAPI at this wavelength. Furthermore, this material has a very wide bandgap of greater than 5 eV, meaning that it is transparent into the mid-ultraviolet and mitigates two photon absorption down to an operation wavelength of 500 nm. Furthermore, the material has a high laser induced damage threshold (LIDT), thus, promising to be an excellent platform for nonlinear optics in both the visible and near-IR wavelength regions.

# Results

Metal-free perovskite films of DNI and MDNI were deposited to a thickness of 500 nm onto thin silica substrates via single source evaporation of pre-synthesized crystalline powders. Each powder was derived by the cooling of a saturated equimolar solution that consisted of the requisite cation iodides and hydroiodic acid. This approach for film deposition is a greatly simplified analogue of the well established, and far more complex, dual-source evaporation process that is required to deposit the state-of-the-art lead-based perovskite material.[25–27] Remarkably, this simple deposition method yields very uniform and pinhole-free films that have a highly transparent glass-like appearance, as shown in Figure 2a. The relative simplicity of the approach holds great potential for the integration of the metal-free perovskite materials family with other materials systems. To investigate the promise of the materials for nonlinear optical applications, their structural and optical properties were examined.

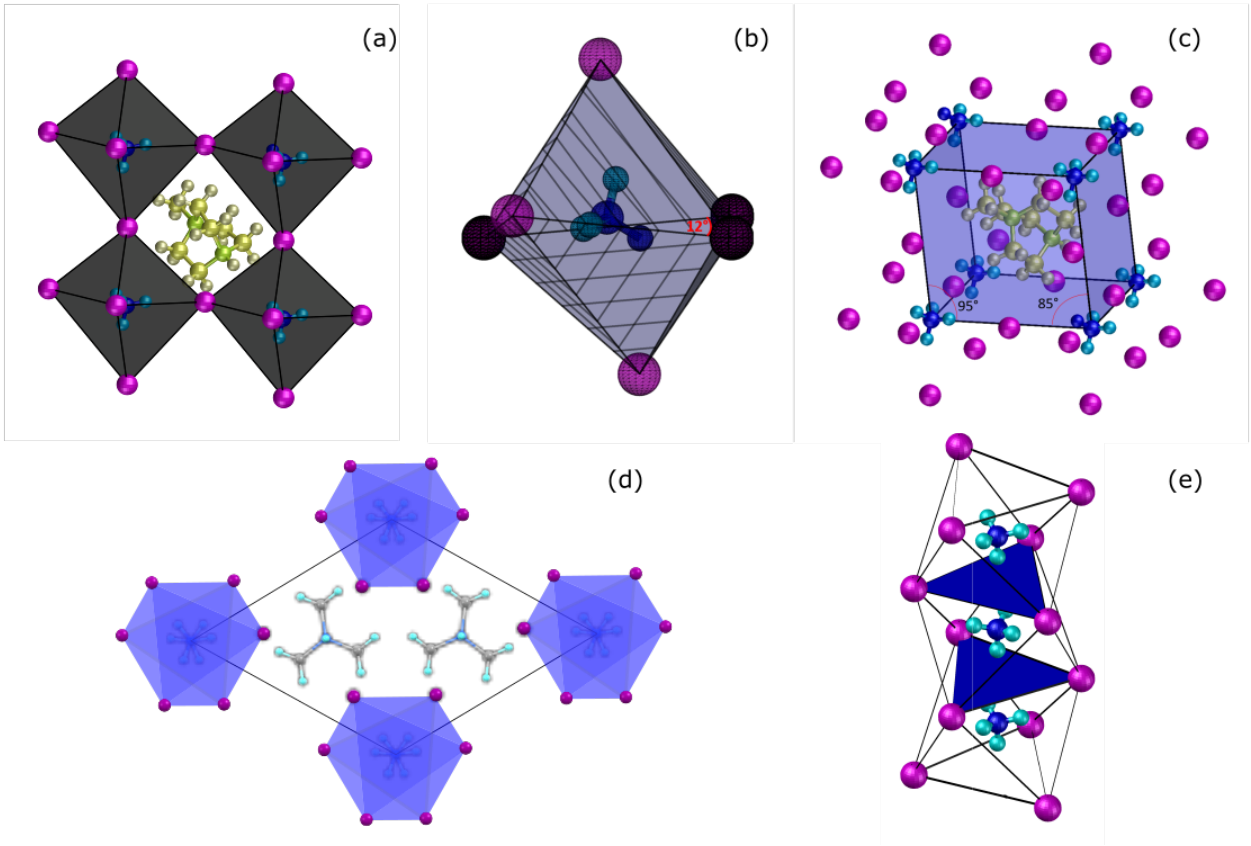


Figure 1: MDNI crystal packing with a) side view highlighting the distortion of the $NH_4I_6$ octahedra, b) distortion of the $NH_4I_6$ octahedra, c) position of MDABCO dication in the distorted cube formed by ammonium cations. d) DNI crystal packing structure, e) 1D column of face-sharing octahedra in the DNI crystal. Colour codes: $MDABCO^{2+}$ - yellow, DABCO - sky blue and grey, $NH_4^+$ - blue, $I^-$ - purple, MNDI octahedra faces - grey, DNI octahedra faces - blue.

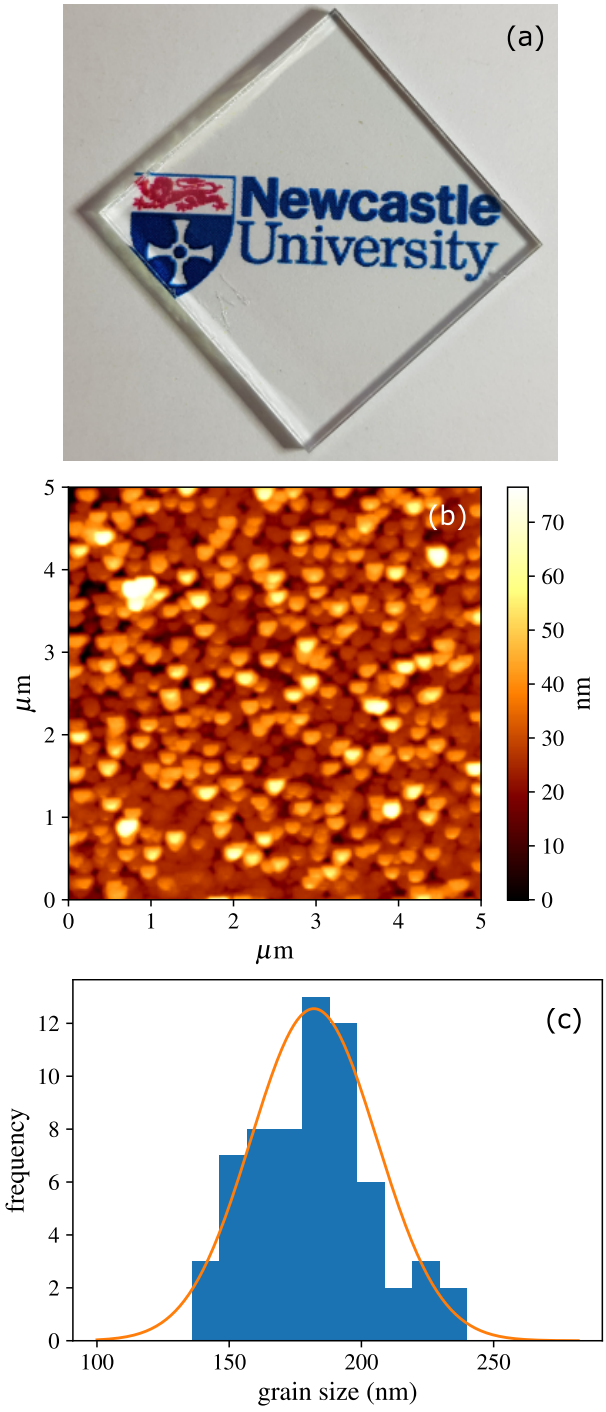


Figure 2: a) A substrate with a 500 nm as-deposited MDNI film (logo used with permission of Newcastle University) b) AFM image of the as evaporated MDNI film. c) Histogram of the grain size – sampled from b).

## Materials Characterization – structural

The grain size and surface roughness of the as-deposited films were measured using an atomic force microscope and the results are shown in Figure 2b. A statistical sample, see Figure 2c, of the grains was used to determine that the median grain size was 180 nm with a standard deviation of 20 nm. The standard deviation indicates a low distribution of grain sizes and the results were very similar for both the DNI and MDNI films, which suggests that the deposition quality is independent of the cation. The surface roughness was determined to be 10 nm RMS and this value is commensurate with other evaporated poly-crystalline materials.[28] Smooth films are critical for optical applications as they reduce scattering and increase the material's optical damage threshold. It is noted that the material can be grown in single crystal form and that it can be polished to improve the roughness value.

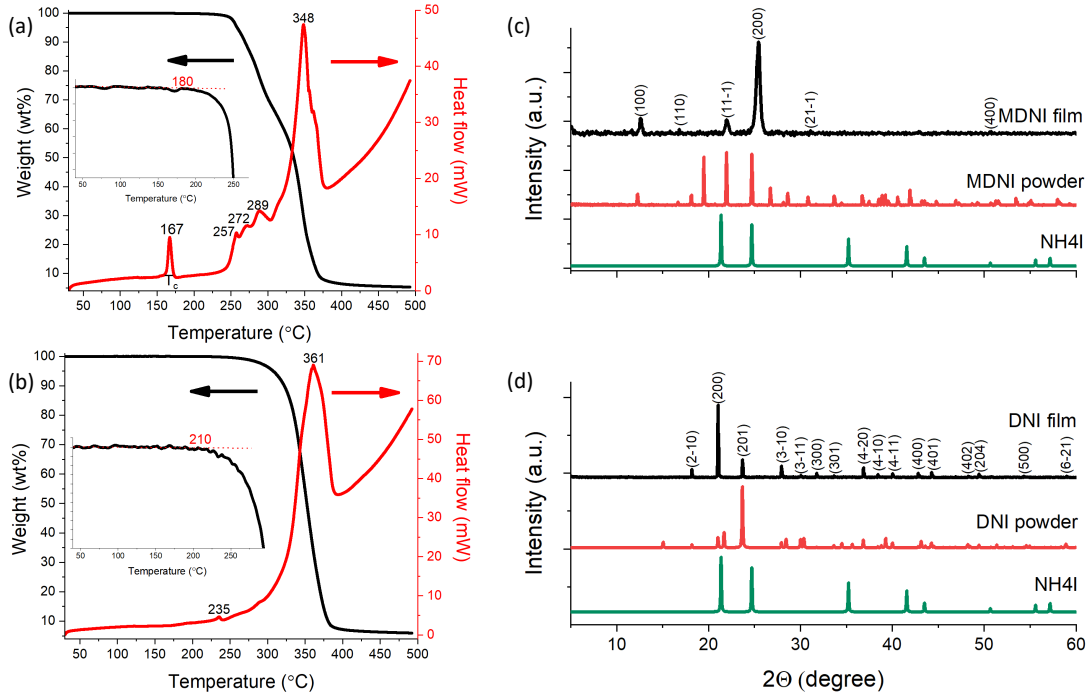


Figure 3: a) TGA and DSC of MDNI film. b) TGA and DSC of DNI film. c) XRD of MDNI produced with a single source evaporation and the corresponding source powder. d) XRD of DNI film produced with a single source evaporation and the corresponding source powder. The XRD of an $NH_4I$ film is included in c) and d) for reference.

Thermogravimetric analysis (TGA) and differential scanning calorimetry (DSC) mea-

surements were performed to determine the thermal stability of materials and the suitable evaporation temperature range, with the results presented in Figures 3a and b. Firstly, it should be noted that MDNI shows a high ferroelectric to paraelectric phase transition temperature $T_c$ of 167 °C, much higher than that reported for MAPI, 57 °C.[29,30] At temperatures above 180 °C MDNI shows the onset of thermal decomposition with the first DSC peak at 257 °C. In the case of DNI, the phase transition occurs above the decomposition onset temperature of 210 °C. To avoid secondary phases in the evaporated films, the temperature of source material was kept below 165 °C.

In order to identify the material phases in the deposited films, they were subjected to X-ray diffraction (XRD), as shown in Figures 3c and d, and compared to the source materials and the theoretical XRD spectra, which were calculated using the crystallographically determined structures, see Figures 3c and d and Figures S1, S2 and S3 (supplementary information). In the case of DNI, all the XRD peaks can be attributed to the P62c phase of the DNI perovskite. The XRD peaks for the MDNI film correspond to the ferroelectric R3 phase whilst the paraelectric phase P432 was not detected. The R3 phase is associated with a strong distortion of the iodide octahedra (Figure 1c) producing a strong dipole moment, as compared to the more symmetrical P432 phase.[31] Additionally, we note a strain along the [100] plane in the evaporated films of MDNI that corresponds to about 2% compression in the d-spacing.

## Materials Characterization – optical

UV-Vis absorption spectra were taken for both the DNI and MDNI films and these were used to create the Tauc plots shown in Figure 4. The squared-exponent form of the Tuac plot was used and the characteristic features of a direct bandgap semiconductor are evident for both plots. For nonlinear optics a direct bandgap can be beneficial as the lack of phonon assisted recombination permits a stronger LIDT when absorption and higher-order absorption effects are present. As expected, at low photon energies both of the materials are highly transparent

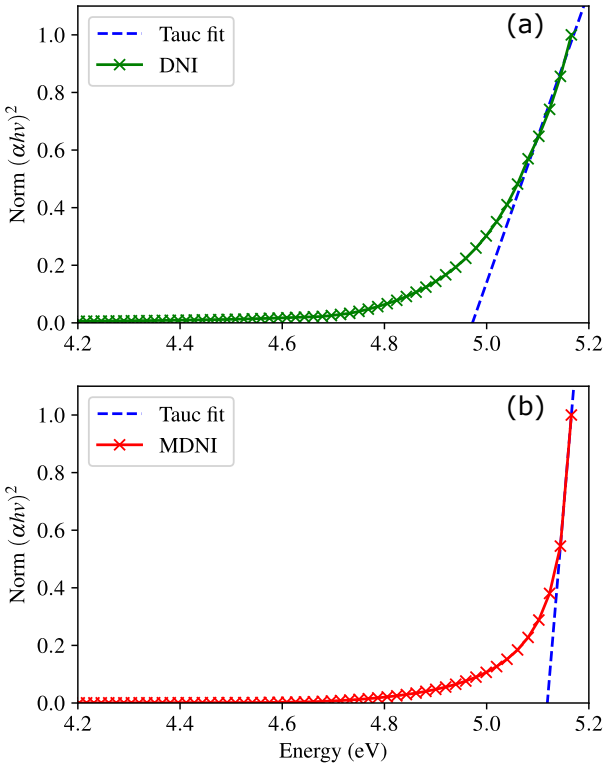


Figure 4: Tauc plot from UV-Vis analysis of a) DNI, and b) MDNI films evaporated from a single source.

and the absorption gets stronger as the bandgap energy is approached. Photons with higher energies are strongly absorbed as they have energy that exceeds that required to excite an electron from the valence band to the conduction band. In this region of the Tauc plots, linear fits were extrapolated to the $x$-axis intercept to find the bandgap energy values for each material. The DNI was measured to have a bandgap value of 4.97 eV and the MDNI was determined to have a slightly larger bandgap of 5.12 eV. Both of these values are much greater than for the standard lead halide perovskite materials and this implies a much broader range of transparency for nonlinear optical applications in the visible and near-IR.[24] Though density functional theory is poor at predicting bandgap values, previous work, by Cui *et al*, has indicated that the valence band maximum mainly originates from the $5p$ orbital of I, while the conduction band minimum is dominated by the cation.[32] In their work, the conduction band did not change significantly when the cation (DABCO) was used in conjunction with different halides, so it is likely that this slight difference in bandgap is dominated by the change in cation. The Tauc plots were analyzed using the 'Near-Edge Absorptivity Ratio', NEAR, method to quantify the magnitude of the Urbach tail and give an indication of the density of sub-gap energy absorbing defect states.[33] The NEAR for the DNI and MDNI were measured to be 0.48 and 0.22, respectively, which indicates low sub-gap absorption and a 'sharp' band-edge. The value for MDNI can be considered exceptional for a thin film and predicts excellent optical transparency at photon energies below and approaching its bandgap energy.[33] An inteferometric approach was used to determine the refractive index of both materials at a wavelength of 1060 nm and the values of 1.68 and 1.62 were obtained for DNI and MDNI respectively. This is significantly lower than that for MAPI at this wavelength, 2.2, which is a potential advantage for metal-free perovskites, as this equates to approximately 10% lower input Fresnel reflection losses for a nonlinear optical component.

The $z$-scan technique is a well established measurement for the accurate determination of the third-order nonlinear optical properties of bulk materials. The process involves translat-

ing the sample through the focus of a single collimated excitation beam. The beam intensity increases as the sample approaches the focal point and the intensity-sensitive nonlinear response is logged as a function of the sample's position. The process allows for both the nonlinear intensity-dependent absorption, $\beta$, and refraction, $n_2$, of the films to be measured simultaneously.

There are two schemes typically used for the $z$-scan measurement, the closed-aperture and open-aperture schemes. The closed-aperture scheme uses a small aperture to spatially filter the signal at the photodetector and this causes the signal to be sensitive to both the nonlinear refraction and the nonlinear absorption.[34,35] The normalised transmission, $T$, measured by the closed-aperture $z$-scan, can be fit with Equation (1), where $z$ is the scan distance from the focal point, $z_0$ is the Rayleigh length of the focusing lens, $S$ is the aperture transmittance, $L_{eff}$ is the effective sample thickness, $I_0$ is the intensity at the focus and $\lambda$ is the incident wavelength, which in this experiment is 1060 nm.[36,37] The open-aperture configuration measures just the intensity-dependant absorption of the sample and this can be fit in isolation using Equation (1) with the aperture transmittance set to $S = 1$. If sufficient, this absorption can cause other refractive index changes in the material via plasma dispersion and thermal lensing effects. It is important to monitor the nonlinear absorption as it can cause large errors to the measurement of a material's $n_2$. These errors can be minimized by setting the excitation laser parameters to a low repetition rate and a pulse duration in the ultrafast regime. In this work, the repetition rate of the laser was set at 1 kHz and the pulse duration set to 300 fs. In addition, each experiment was repeated with the pulse duration extended to 3 ps to ensure that the measurement of the $n_2$ was isolated from the other refractive index modulating effects.

$$T = 1 - \frac{8\pi}{\lambda\sqrt{2}} \frac{(z/z_0)\,(1-S)^{0.25}\, L_{eff} n_2 I_0}{\left(1+(z/z_0)^2\right)\left(9+(z/z_0)^2\right)} + \frac{1}{2\sqrt{2}} \frac{\beta L_{eff} I_0\,(z/z_0)^2}{\left(1+(z/z_0)^2\right)\left(9+(z/z_0)^2\right)} \qquad (1)$$

Closed and open-aperture $z$-scan measurements were taken of the DNI and MDNI samples

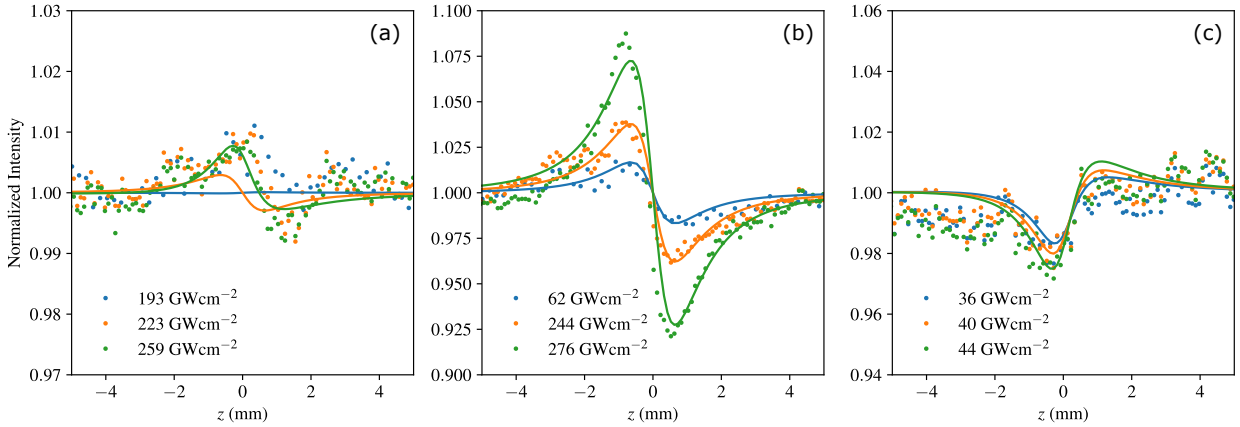


Figure 5: Closed-aperture $z$-scan of a) DNI b) MDNI c) MAPI. Dots are the measured data and the lines represent the data fit using Equation 1.

at a range of laser powers. For comparison and bench-marking purposes, a further set of measurements were performed on a film of the archetypal MAPI perovskite. The closed-aperture measurements are presented in Figure 5 and it is immediately obvious that all three samples show the 'peak-valley' signal that is typical of nonlinear refraction. Equation (1) was fit to the data using a least squares algorithm with the nonlinear refraction and the nonlinear absorption initialised as free parameters. The fittings are also shown in Figure 5 and the values returned for the $n_2$ were $3 \times 10^{-18}\,\mathrm{m^2\,W^{-1}}$ for the DNI and $5.7 \times 10^{-17}\,\mathrm{m^2\,W^{-1}}$ for the MDNI, so that there is an order of magnitude difference. It is noted that the $z$-scan apparatus did not detect a discernible signal from the DNI sample at excitation intensities lower than $200\,\mathrm{GW\,cm^{-2}}$. However, once a signal could be detected, the measured $n_2$, for each sample, did not change as a function of intensity and this is a strong indication that plasma dispersion and thermal lensing were avoided. In agreement with dispersion models for the nonlinear refractive index, at the wavelength of measurement the nonlinear refractive index of MAPI is negative.[38] This nonlinear refractive index is predicted to be negative when $\hbar\omega/E_g > 0.7$ and for the MAPI measurement $\hbar\omega/E_g = 0.74$. The nonlinear refractive index of the MAPI was determined to be $-5.8 \times 10^{-17}\,\mathrm{m^2\,W^{-1}}$, which whilst opposite in sign to the DABCO materials, but commensurate in magnitude with MDNI. However, at higher powers, the nonlinear refractive index of the MAPI decreases; an indication that the

nonlinear absorption and associated free carrier and thermal induced effects dominate the measurement. This is illustrated by the asymmetry of the 'peak-valley' signal at the higher powers. To minimise this contribution, the reported values for the nonlinear properties are taken from the lower power measurements where the value for the $n_2$ is unchanged. The MAPI sample could not be measured at intensities greater than $45\,\mathrm{GW\,cm^{-2}}$ as the laser intensity damaged the material.

The open-aperture $z$-scan measurements with the corresponding fits generated using Equation 1 ($S = 1$) are shown in Figure 6 and these clearly support our analysis of the close-aperture results. The DNI and MDNI samples show no evidence of multi-photon absorption and the $\beta$ was effectively zero for both samples. This is expected, as the very wide bandgap of these materials means that no two-photon absorption is expected for excitation wavelengths above 500 nm, which makes them very useful for frequency conversion applications in the visible regime. In contrast, the MAPI shows a strong nonlinear absorption coefficient of $1.2 \times 10^{-9}\,\mathrm{m\,W^{-1}}$. To put these values into context, at the operation wavelength used in these studies, $As_2S_3$, which is considered an excellent material for third-order nonlinear optics and is one of the best-known wide bandgap (2.4 eV) chalcogenide glasses, has an $n_2 = 4.3 \times 10^{-18}\,\mathrm{m^2\,W^{-1}}$ with negligible two photon absorption.[39,40]

A consequence of strong nonlinear absorption is that it reduces the efficiency of nonlinear refraction. Thus, there is a balance between both parameters that will determine the potential of a material for nonlinear applications. It is, therefore, instructive to determine a nonlinear figure of merit, $FOM_{nl}$, to compare different materials for nonlinear applications at a specific wavelength. The $FOM_{nl}$ is given by Equation 2.[40,41]

$$FOM_{nl} = \frac{n_2}{\beta\lambda} \tag{2}$$

To calculate the $FOM_{nl}$ for the MDNI and DNI samples, $\beta$ was set to $1 \times 10^{-13}\,\mathrm{m\,W^{-1}}$ as this is the resolution limit of our instrument, therefore these values are the lower bound. The $FOM_{nl}$ for these materials, the MAPI, and two other popular lead-based perovskites,

$CH_3NH_2PbBr_3$ (MAPBr) and $CH_3NH_2PbCl_3$ (MAPCl) that were measured are presented in Table 1 and that for MDNI is shown to be four orders of magnitude greater than MAPI and an order of magnitude greater the widest bandgap lead-based perovskite MAPCl. As one would expect, this superior $FOM_{nl}$ is a result of the increased nonlinear refraction and the greatly reduced nonlinear absorption. As the nonlinear absorption is directly correlated with the energy of the excitation photons and the bandgap of the material, it is expected that the DNI and MDNI will have superior $FOM_{nl}$ down to wavelengths of 500 nm ($\hbar\omega = E_g/2$). It is also predicted that the nonlinear refractive index increases when operating at wavelengths slightly longer than the two photon absorption edge. A preliminary set of studies on MDNI at a wavelength of 530 nm, shown in the Supplementary information Figure S5, support this with a five-fold increase in $n_2$ and negligible nonlinear absorption observed. When compared to the wide bandgap $As_2S_3$ and the MAPCl, which have a bandgap greater than twice the photon energy of the the measurement source, the greater $FOM_{nl}$ is predominantly owing to its higher $n_2$. It is noteworthy that the MDNI material has a bandgap more than twice that of $As_2S_3$ and almost twice that of MAPCl. This means that, in comparison, the MDNI is not susceptible to three-photon absorption at the measurement wavelength, which further suppresses multi-photon absorption at high intensities. Furthermore, though the $n_2$ of chalcogenide glasses can be increased by introducing polarizable elements, this also reduces the bandgap energy increasing the propensity for multi-photon absorption.[40]

Table 1: Nonlinear optical properties of MDNI, DNI, MAPI, MAPBr, MAPCl, and $As_2S_3$. * $z$-scan measurements taken at 1150 nm for this material.

| Material | $n_2$ ($m^2\,W^{-1}$) | $\beta$ ($m\,W^{-1}$) | $FOM_{nl}$ | LIDT ($J\,cm^{-2}$) | Type | ref |
|---|---|---|---|---|---|---|
| MDNI | $5.7 \times 10^{-17}$ | $1 \times 10^{-13}$ | $> 537$ | 0.8 | metal-free | this work |
| DNI | $3 \times 10^{-18}$ | $1 \times 10^{-13}$ | $> 28$ | 0.8 | metal-free | this work |
| MAPI | $-5.8 \times 10^{-17}$ | $1.2 \times 10^{-9}$ | 0.05 | 0.01 | lead-based | this work |
| MAPBr | $3.8 \times 10^{-17}$ | $5.3 \times 10^{-10}$ | 0.35 | 0.02 | lead-based | this work |
| MAPCl | $5.8 \times 10^{-18}$ | $1 \times 10^{-13}$ | $> 54$ | 0.03 | lead-based | this work |
| $As_2S_3$* | $4.3 \times 10^{-18}$ | $<1 \times 10^{-12}$ | $> 30$ | 0.02 | arsenic-based | [39,40] |

To be a strong candidate for high-intensity application such as nonlinear optics, a ma-

terial must have a high laser induced damage threshold. Using the same wavelength and pulse parameters as for the $z$-scan measurements, the LIDT for all five films was measured. The results along with the nonlinear optical measurements are summarized in Table 1. The MDNI and the DNI materials have a similar LIDT of $0.8\,\mathrm{J\,cm^{-2}}$, which is almost two orders of magnitude greater than the lead-based perovskites and $As_2S_3$. To give context, the MDNI sample shows an order of magnitude greater phase shift than all of the other perovskite samples, at the point just prior to the LIDT being reached, Figure S6 (supplementary information).

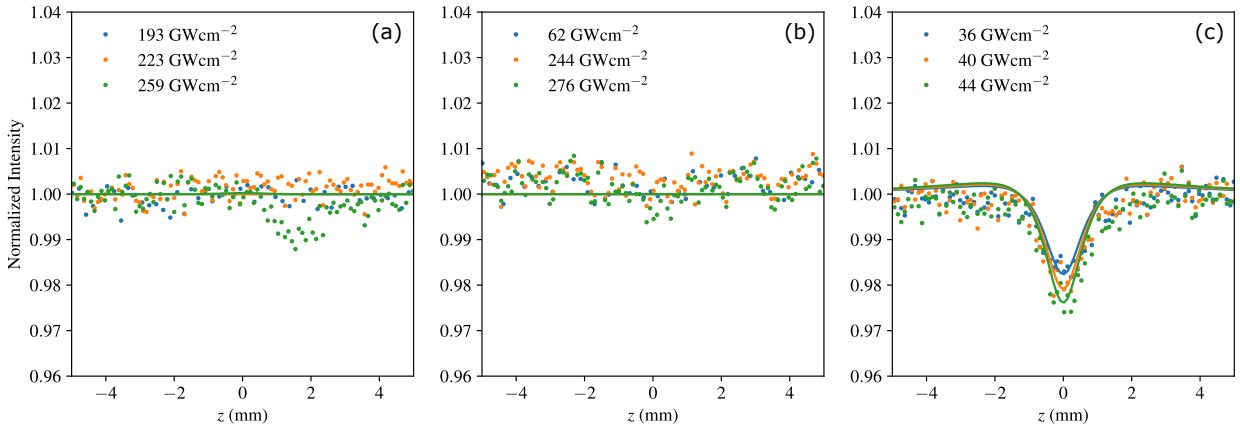


Figure 6: Open-aperture $z$-scan of a) DNI b) MDNI c) MAPI. Dots are the measured data and the lines represent the data fit using Equation 1.

# Conclusion

This work introduces, for the first time, metal-free perovskites as a new class of materials for third-order nonlinear optical processes. Metal-free perovskites are defined as all-organic ionic crystals and as such the nonlinearity is determined by a complex interplay of structural components, i.e. the high second hyperpolarizability of the asymmetric MDABCO cation and the distortion of the ammonium hexaiodide octahedra. Our results show that the non-polar DNI crystal has a high intrinsic third-order nonlinearity and that by replacing the DABCO cation with a polar MDABCO cation, this third-order nonlinearity increases by an order

of magnitude. According to studies of this family of materials for ferroelectrics, the MDNI crystal has alternating $MDABCO^{2+}$ and $NH_4{}^+$ cations along the [111] crystallographic direction.[23] This arrangement produces a resultant polar point group symmetry $C_3$ that induces a spontaneous polarization along that direction. A spontaneous polarization in a lattice implies a lack of inversion symmetry in the bulk material and density functional theory studies have indicated that MDNI as a potential material for second-order processes.[24,42] Though there is no consensus regarding the mechanism for the strong nonlinear refractive index in perovskite materials, our result supports the hypothesis that the third-order nonlinearity can be strengthened when the octahedra are distorted and ionic crystals become asymmetric.[43]

The combination of high laser damage threshold, large $FOM_{nl}$, wide bandgap and associated superior transparency in the important visible and near-IR transmission windows, promise an excellent material for nonlinear optical devices. Furthermore, the non-toxic processing and the abundance of the material's elements greatly expand their scope and potential as candidates for, efficient, inexpensive, and environmentally friendly, nonlinear optics.

# Experimental

## Preparation of samples

1,4-Diazabicyclo[2.2.2]octane (DABCO), $NH_4I$ and HI (57% w/w stabilised with 1.5% $H_3PO_3$) were purchased of the highest purity available and used as received.
N-Methyl-1,4-diazabicyclo[2.2.2]octan-1-ium (MDABCO) iodide was synthesised as described elsewhere.[44,45] Metal halide perovskite films were obtained by using the anti-solvent method described elsewhere.[46,47]

### N-Methyl-1,4-Diazabicyclo[2.2.2]octan-1-ium Ammonium Iodide (MDNI)

0.5 mol MDABCO iodide and ammonium iodide were dissolved in aqueous HI solution (20%, stabilised with 0.5% $H_3PO_3$) at 90 °C. Cooling the pale yellow solution to room temperature resulted in precipitation of white polycrystalline material. Washing with $Et_2O$ and drying in vacuum gave MDNI as a white crystalline solid in 70% yield.

### Substrate preparation

Silica glass substrates were cleaned with 2% solution of Hellmanex in water, and washed with deionized water, acetone and ethanol, and blow-dried with compressed air. Additionally, oxygen plasma was used to clean the glass for 10 minutes prior to the perovskite deposition.

### Evaporation of MDNI

Approximately 50 mg of powdered MDNI was added to a quartz crucible and placed into a tungsten basket heater. The substrates were placed face down at a distance of 30 cm from the source. A density of 2.315 g cm$^{-3}$ was used, as calculated from the crystal structure. The chamber was pumped down to $10^{-6}$ mbar and the source heated to achieve an evaporation rate of approximately 0.3 nm s$^{-1}$. The pressure was maintained above $1 \times 10^{-5}$ mbar during evaporation.

## Characterisation techniques

Perovskite films were evaporated in a BOC-Edwards Auto thermal evaporator. Electronic absorption spectra were recorded at RT using a Shimadzu UV-1800 spectrophotometer. Surface morphology was characterised with AFM in non-contact mode using an XE-150 model from Park Systems equiped with NuNano NuScout 350 tip. X-ray diffraction data were acquired on a Bruker D8 Advance diffractometer in coupled theta / two theta regime.

**$z$-scan**

The incident laser was emitted from a Spectra Physics Spirit One femtosecond laser (wavelength: 1060 nm, pulse duration: 300 fs, repetition rate: 1 kHz). A neutral density filter was used to adjust the intensity on the sample. The lens focal length was 50 mm and the spot size at focal point was 30 µm. The power of the laser was divided by a beamsplitter (8% reflection, 92% transmission). The beam powers were measured by two separated power meters (Thorlabs S120C and S130C) with an aperture ($S = 0.13$) inserted in front of one of the power meters. A schematic of the experimental set-up for the $z$-scan measurements can be found in Figure S4 (supplementary information).

# Supporting Information Available

The Supporting Information is available free of charge at
X-ray diffraction of MDNI and DNI, schematic of $z$-scan measurement technique, measurements of maximum phase shift for all materials under investigation, z-scan of MDNI at 530 nm wavelength.

# Acknowledgement

The authors acknowledge the Engineering and Physical Sciences Research Council, EPSRC, (EP/S031103/1 & EP/T010568/1) for financial support.

# References

(1) Arora, N.; Dar, M. I.; Hinderhofer, A.; Pellet, N.; Schreiber, F.; Zakeeruddin, S. M.; Grätzel, M. Perovskite solar cells with CuSCN hole extraction layers yield stabilized efficiencies greater than 20%. *Science* **2017**, *358*, 768–771.

(2) Sadhanala, A.; Ahmad, S.; Zhao, B.; Giesbrecht, N.; Pearce, P. M.; Deschler, F.; Hoye, R. L.; Gödel, K. C.; Bein, T.; Docampo, P., et al. Blue-green color tunable solution processable organolead chloride–bromide mixed halide perovskites for optoelectronic applications. *Nano Lett.* **2015**, *15*, 6095–6101.

(3) Amat, A.; Mosconi, E.; Ronca, E.; Quarti, C.; Umari, P.; Nazeeruddin, M. K.; Grätzel, M.; De Angelis, F. Cation-induced band-gap tuning in organohalide perovskites: interplay of spin–orbit coupling and octahedra tilting. *Nano Lett.* **2014**, *14*, 3608–3616.

(4) Jang, D. M.; Park, K.; Kim, D. H.; Park, J.; Shojaei, F.; Kang, H. S.; Ahn, J.-P.; Lee, J. W.; Song, J. K. Reversible halide exchange reaction of organometal trihalide perovskite colloidal nanocrystals for full-range band gap tuning. *Nano Lett.* **2015**, *15*, 5191–5199.

(5) Xu, J.; Li, X.; Xiong, J.; Yuan, C.; Semin, S.; Rasing, T.; Bu, X.-H. Halide perovskites for nonlinear optics. *Adv. Mater.* **2020**, *32*, 1806736.

(6) Zhou, Y.; Huang, Y.; Xu, X.; Fan, Z.; Khurgin, J. B.; Xiong, Q. Nonlinear optical properties of halide perovskites and their applications. *Appl. Phys. Rev.* **2020**, *7*, 041313.

(7) Han, X.; Zheng, Y.; Chai, S.; Chen, S.; Xu, J. 2D organic-inorganic hybrid perovskite materials for nonlinear optics. *Nanophotonics* **2020**, *9*, 1787–1810.

(8) Zhou, F.; Ran, X.; Fan, D.; Lu, S.; Ji, W. Perovskites: Multiphoton Absorption and Applications. *Adv. Opt. Mater.* **2021**, 2100292.

(9) Chen, W.; Zhang, F.; Wang, C.; Jia, M.; Zhao, X.; Liu, Z.; Ge, Y.; Zhang, Y.; Zhang, H. Nonlinear Photonics Using Low-Dimensional Metal-Halide Perovskites: Recent Advances and Future Challenges. *Adv. Mater.* **2021**, *33*, 2004446.

(10) Franken, P. A.; Hill, A. E.; Peters, C. W.; Weinreich, G. Generation of Optical Harmonics. *Phys. Rev. Lett.* **1961**, *7*, 118–119.

(11) Kalanoor, B. S.; Gouda, L.; Gottesman, R.; Tirosh, S.; Haltzi, E.; Zaban, A.; Tischler, Y. R. Third-Order Optical Nonlinearities in Organometallic Methylammonium Lead Iodide Perovskite Thin Films. *ACS Photonics* **2016**, *3*, 361–370.

(12) Zhang, R.; Fan, J.; Zhang, X.; Yu, H.; Zhang, H.; Mai, Y.; Xu, T.; Wang, J.; Snaith, H. J. Nonlinear Optical Response of Organic–Inorganic Halide Perovskites. *ACS Photonics* **2016**, *3*, 371–377.

(13) Suárez, I.; Vallés-Pelarda, M.; Gualdrón-Reyes, A. F.; Mora-Seró, I.; Ferrando, A.; Michinel, H.; Salgueiro, J. R.; Pastor, J. P. M. Outstanding nonlinear optical properties of methylammonium- and Cs-PbX3 (X = Br, I, and Br–I) perovskites: Polycrystalline thin films and nanoparticles. *APL Mater.* **2019**, *7*, 041106.

(14) Yi, J.; Miao, L.; Li, J.; Hu, W.; Zhao, C.; Wen, S. Third-order nonlinear optical response of CH3NH3PbI3 perovskite in the mid-infrared regime. *Opt. Mater. Express* **2017**, *7*, 3894–3901.

(15) Ganeev, R. A.; Rao, K. S.; Yu, Z.; Yu, W.; Yao, C.; Fu, Y.; Zhang, K.; Guo, C. Strong nonlinear absorption in perovskite films. *Opt. Mater. Express* **2018**, *8*, 1472–1483.

(16) Song, Z.; Abate, A.; Watthage, S. C.; Liyanage, G. K.; Phillips, A. B.; Steiner, U.; Graetzel, M.; Heben, M. J. In-situ observation of moisture-induced degradation of perovskite solar cells using laser-beam induced current. IEEE Photovoltaic Spec. Conf., 43rd. 2016; pp 1202–1206.

(17) Ruan, S.; Surmiak, M.-A.; Ruan, Y.; McMeekin, D. P.; Ebendorff-Heidepriem, H.; Cheng, Y.-B.; Lu, J.; McNeill, C. R. Light induced degradation in mixed-halide perovskites. *J. Mater. Chem. C* **2019**, *7*, 9326–9334.

(18) Babayigit, A.; Ethirajan, A.; Muller, M.; Conings, B. Toxicity of organometal halide perovskite solar cells. *Nat. Mater.* **2016**, *15*, 247.

(19) Babayigit, A.; Thanh, D. D.; Ethirajan, A.; Manca, J.; Muller, M.; Boyen, H.-G.; Conings, B. Assessing the toxicity of Pb-and Sn-based perovskite solar cells in model organism Danio rerio. *Sci. Rep.* **2016**, *6*, 1–11.

(20) Ke, W.; Kanatzidis, M. G. Prospects for low-toxicity lead-free perovskite solar cells. *Nat. Commun.* **2019**, *10*, 965.

(21) Billen, P.; Leccisi, E.; Dastidar, S.; Li, S.; Lobaton, L.; Spatari, S.; Fafarman, A. T.; Fthenakis, V. M.; Baxter, J. B. Comparative evaluation of lead emissions and toxicity potential in the life cycle of lead halide perovskite photovoltaics. *Energy* **2019**, *166*, 1089–1096.

(22) Tsai, S.-M.; Mesina, M.; Goshia, T.; Chiu, M.-H.; Young, J.; Sibal, A.; Chin, W.-C. Perovskite nanoparticles toxicity study on airway epithelial cells. *Nanoscale Res. Lett.* **2019**, *14*, 1–8.

(23) Ye, H.-Y.; Tang, Y.-Y.; Li, P.-F.; Liao, W.-Q.; Gao, J.-X.; Hua, X.-N.; Cai, H.; Shi, P.-P.; You, Y.-M.; Xiong, R.-G. Metal-free three-dimensional perovskite ferroelectrics. *Science* **2018**, *361*, 151–155.

(24) Kasel, T. W.; Deng, Z.; Mroz, A. M.; Hendon, C. H.; Butler, K. T.; Canepa, P. Metal-free perovskites for non linear optical materials. *Chem. Sci.* **2019**, *10*, 8187–8194.

(25) Liu, M.; Johnston, M. B.; Snaith, H. J. Efficient planar heterojunction perovskite solar cells by vapour deposition. *Nature* **2013**, *501*, 395–398.

(26) Wang, S.; Li, X.; Wu, J.; Wen, W.; Qi, Y. Fabrication of efficient metal halide perovskite solar cells by vacuum thermal evaporation: A progress review. *Curr. Opin. Electrochem.* **2018**, *11*, 130–140.

(27) Dubey, A.; Adhikari, N.; Mabrouk, S.; Wu, F.; Chen, K.; Yang, S.; Qiao, Q. A strategic review on processing routes towards highly efficient perovskite solar cells. *J. Mater. Chem. A* **2018**, *6*, 2406–2431.

(28) Michael, A.; Kwok, C. Y. Evaporated Thick Polysilicon Film With Low Stress and Low Thermal Budget. *J. Microelectromech. Syst.* **2013**, *22*, 825–827.

(29) Whitfield, P.; Herron, N.; Guise, W.; Page, K.; Cheng, Y.; Milas, I.; Crawford, M. Structures, phase transitions and tricritical behavior of the hybrid perovskite methyl ammonium lead iodide. *Sci. Rep.* **2016**, *6*, 1–16.

(30) Rakita, Y.; Bar-Elli, O.; Meirzadeh, E.; Kaslasi, H.; Peleg, Y.; Hodes, G.; Lubomirsky, I.; Oron, D.; Ehre, D.; Cahen, D. Tetragonal CH3NH3PbI3 is ferroelectric. *Proc. Natl. Acad. Sci. U.S.A.* **2017**, *114*, E5504–E5512.

(31) Wang, H.; Liu, H.; Zhang, Z.; Liu, Z.; Lv, Z.; Li, T.; Ju, W.; Li, H.; Cai, X.; Han, H. Large piezoelectric response in a family of metal-free perovskite ferroelectric compounds from first-principles calculations. *Npj Comput. Mater.* **2019**, *5*, 1–9.

(32) Cui, Q.; Song, X.; Liu, Y.; Xu, Z.; Ye, H.; Yang, Z.; Zhao, K.; Liu, S. F. Halide-modulated self-assembly of metal-free perovskite single crystals for bio-friendly X-ray detection. *Matter* **2021**,

(33) Viezbicke, B. D.; Patel, S.; Davis, B. E.; Birnie III, D. P. Evaluation of the Tauc method for optical absorption edge determination: ZnO thin films as a model system. *Phys. Status Solidi B* **2015**, *252*, 1700–1710.

(34) Sheik-Bahae, M.; Said, A. A.; Wei, T. .; Hagan, D. J.; Van Stryland, E. W. Sensitive measurement of optical nonlinearities using a single beam. *IEEE J. Quantum Electron.* **1990**, *26*, 760–769.

(35) de Araújo, C. B.; Gomes, A. S. L.; Boudebs, G. Techniques for nonlinear optical characterization of materials: a review. *Rep. Prog. Phys.* **2016**, *79*, 036401.

(36) Dinu, M.; Quochi, F.; Garcia, H. Third-order nonlinearities in silicon at telecom wavelengths. *Appl. Phys. Lett.* **2003**, *82*, 2954–2956.

(37) Bristow, A. D.; Rotenberg, N.; van Driel, H. M. Two-photon absorption and Kerr coefficients of silicon for 850–2200nm. *Appl. Phys. Lett.* **2007**, *90*, 191104.

(38) Sheik-Bahae, M.; Hutchings, D. C.; Hagan, D. J.; Van Stryland, E. W. Dispersion of bound electron nonlinear refraction in solids. *IEEE J. Quantum Electron.* **1991**, *27*, 1296–1309.

(39) Zhang, M.; Li, T.; Yang, Y.; Tao, H.; Zhang, X.; Yuan, X.; Yang, Z. Femtosecond laser induced damage on Ge-As-S chalcogenide glasses. *Opt. Mater. Express* **2019**, *9*, 555–561.

(40) Wang, T.; Gai, X.; Wei, W.; Wang, R.; Yang, Z.; Shen, X.; Madden, S.; Luther-Davies, B. Systematic z-scan measurements of the third order nonlinearity of chalcogenide glasses. *Opt. Mater. Express* **2014**, *4*, 1011–1022.

(41) Ferrando, A.; Martínez Pastor, J. P.; Suárez, I. Toward Metal Halide Perovskite Nonlinear Photonics. *J. Phys. Chem. Lett.* **2018**, *9*, 5612–5623.

(42) Denev, S. A.; Lummen, T. T. A.; Barnes, E.; Kumar, A.; Gopalan, V. Probing Ferroelectrics Using Optical Second Harmonic Generation. *J. Am. Ceram. Soc.* **2011**, *94*, 2699–2727.

(43) Zhang, R.; Fan, J.; Zhang, X.; Yu, H.; Zhang, H.; Mai, Y.; Xu, T.; Wang, J.; Snaith, H. J. Nonlinear optical response of organic–inorganic halide perovskites. *ACS Photonics* **2016**, *3*, 371–377.

(44) Vasilev, A.; Deligeorgiev, T.; Gadjev, N.; Drexhage, K.-H. Synthesis of novel monomeric and homodimeric cyanine dyes based on oxazolo [4, 5-b] pyridinium and quinolinium end groups for nucleic acid detection. *Dyes Pigm.* **2005**, *66*, 135–142.

(45) Kurutos, A.; Orehovec, I.; Saftić, D.; Horvat, L.; Crnolatac, I.; Piantanida, I.; Deligeorgiev, T. Cell penetrating, mitochondria targeting multiply charged DABCO-cyanine dyes. *Dyes Pigm.* **2018**, *158*, 517–525.

(46) Schultes, M.; Giesbrecht, N.; Kuffner, J.; Ahlswede, E.; Docampo, P.; Bein, T.; Powalla, M. Universal nanoparticle wetting agent for upscaling perovskite solar cells. *ACS Appl. Mater. Interfaces* **2019**, *11*, 12948–12957.

(47) Petrus, M. L.; Hu, Y.; Moia, D.; Calado, P.; Leguy, A. M.; Barnes, P. R.; Docampo, P. The influence of water vapor on the stability and processing of hybrid perovskite solar cells made from non-stoichiometric precursor mixtures. *ChemSusChem* **2016**, *9*, 2699–2707.

# Graphical TOC Entry

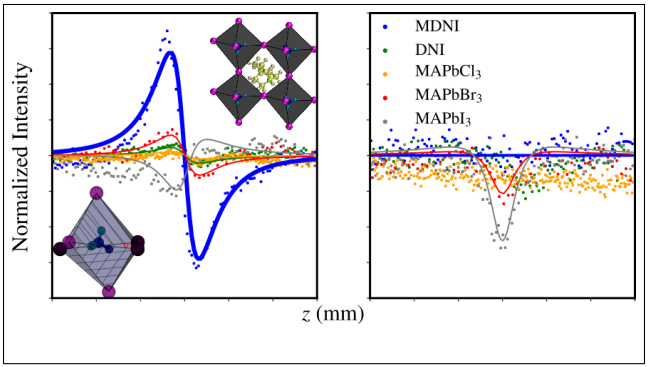


**For Table of Contents Use Only**
A wide bandgap metal-free perovskite for third-order nonlinear optics.

Dumitru Sirbu, Hei Chit Leo Tsui,* Naseem Alsaif, Susana Iglesias-Porras, Yifeng Zhang, Ming Wang, Mingzhen Liu, Anna C. Peacock, Pablo Docampo, and Noel Healy.

Image shows the enhanced nonlinear response and negligible non-linear absorption for a MDNI crystal. Inset are the crystal structure and the associated distorted octahedron that plays an important role in the nonlinearity.